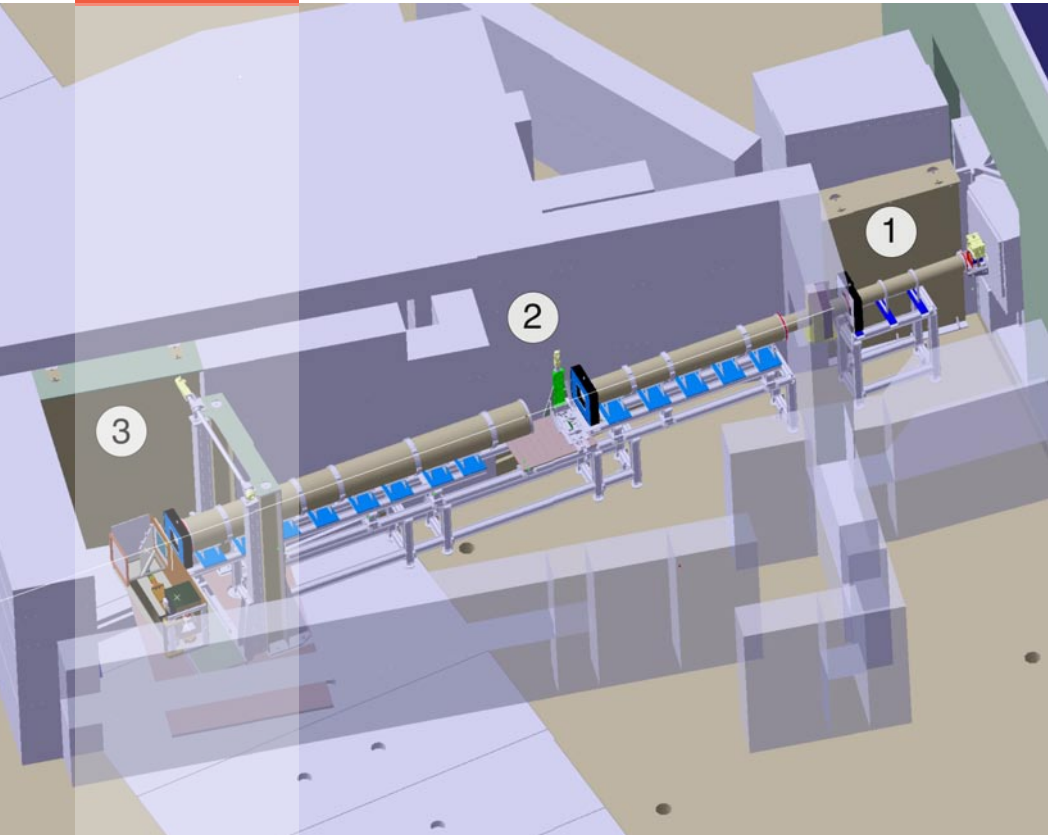
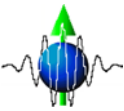


# SWISS NEUTRON NEWS



Schweizerische Gesellschaft für Neutronenstreuung  
Société Suisse pour la Diffusion des Neutrons  
Swiss Neutron Scattering Society

## Editorial:

Editor: Swiss Neutron Scattering Society

Board for the Period January 2004 – January 2007:

President: Dr. P. Allenspach peter.allenspach@psi.ch  
Board Members: Prof. Dr. S. Decurtins silvio.decurtins@iac.unibe.ch  
Prof. Dr. B. Schönfeld schoenfeld@iap.phys.ethz.ch  
Secretary: Dr. S. Janssen stefan.janssen@psi.ch

Honorary Members: Prof. Dr. W. Hälg, ETH Zürich  
Prof. Dr. K.A. Müller, IBM Rüschlikon and Univ. Zürich  
Prof. Dr. A. Furrer, ETH Zürich and Paul Scherrer Institut

Revisers: Dr. W. Fischer, Paul Scherrer Institut  
Dr. K. Krämer, University of Berne

Address: Sekretariat SGN/SSDN  
Paul Scherrer Institut  
bldg. WLGA/002  
5232 Villigen PSI, Switzerland  
phone: +41-(0)56 - 310 4666  
fax: +41-(0)56 - 310 3294  
www: <http://sgn.web.psi.ch>

Bank Account: 50-70723-6

Printing: Paul Scherrer Institut

Circulation: 1900, 2 numbers per year

Copyright: SGN/SSDN and the respective authors

### ***On the cover:***

*On October 14, 2005 the SINQ cold neutron radiography facility 'ICON' was inaugurated on the occasion of an international workshop on 'Neutron Imaging Using Cold Neutrons' at PSI. The new instrument is featured in detail by an article within this issue of Swiss Neutron News.*

*The cover illustration shows a view into the ICON bunker: Nr. 1 shows the inner bunker, where a velocity selector, filters and other equipments can be inserted into the flight path of neutrons. Nr. 2 and 3 are the standard experimental positions. At the position Nr. 2 small and light probes can be examined (e.g. micro-tomography), where at position Nr. 3 bigger and heavier probes can be scanned through the neutron beam.*

# *Contents*

---

page

<b>The President's Page.....</b>	<b>2</b>
<b>Data Reduction on Time-of-Flight Instruments .....</b>	<b>4</b>
<b>Dynamic Rotational Anion Disorder in Tetrahydroxoborate Sodalite Investigated by Quasielastic Neutron Scattering .....</b>	<b>13</b>
<b>ICON – The New Facility for Cold Neutron Imaging at the Swiss Spallation Neutron Source SINQ .....</b>	<b>20</b>
<b>Albert Furrer and Hans Ulrich Güdel received the 2005 ENSA Walter Hälg Prize .....</b>	<b>30</b>
<b>ENSA Press Release .....</b>	<b>33</b>
<b>Announcements .....</b>	<b>35</b>
<b>4<sup>th</sup> PSI Summer School in Zuoz 2005 .....</b>	<b>37</b>
<b>Day of Physics at PSI .....</b>	<b>39</b>
<b>Conferences 2006 .....</b>	<b>40</b>
<b>SGN/SSDN – Registration Form .....</b>	<b>43</b>

## *The President's Page*



Dear members

It is a great pleasure for me and a great honor for our society that two of its eminent members, Albert Furrer and Hans Ulrich Güdel, have been awarded the „2005 Walter Hälgl Prize“ of the European Neutron Scattering Association (ENSA). First and foremost I would like to congratulate the two prize winners in the name of SGN/SNSS for this prestigious prize but also for their dedication to neutron scattering. Their names are intimately linked to the successful development of neutron scattering and its utilization in Switzerland and the present, very strong standing of Swiss neutron scattering on an inter-

national scale. Albert and Hans Ueli were co-founders of SGN/SNSS, Albert as its first chairman and Hans Ueli as a board member. You will find a laudation by Joël Mesot in this issue listing their scientific achievements. It is amazing to see in how many research fields their collaboration had and still has a decisive impact and I am looking forward to their future experiments and publications.

The installation of the liquid metal target Megapie into SINQ during the first half of 2006 will mark a major step in the target development. It is a very complex and demanding project to assure a safe and successful operation of this target. However, the people involved in the Megapie development have carefully tried to exclude any eventualities by putting several layers of security measures in place and by testing the set-up on a test rig. Hence, everything possible was done to guarantee a successful operation, but even in the optimum case it will have a severe effect for the SINQ users: The operation of the instruments in 2006 will be several months shorter than usual and the reliability of the beam in the second half of the year might be a problem. For more information concerning proposal deadlines and operation schedule, please consult the „announcements page“ in this issue.

In early summer 2006 the first neutrons are planned to be produced at the 3<sup>rd</sup> generation neutron source SNS in Oak Ridge, USA. Judging from the excellent track record of this project as far as being within the time limit and being within the budget are concerned, I have no doubt that this goal will be reached. Of course, it will take some time to ramp the power up to the design value and to transform the instruments into

really user friendly machines, including appropriate sample environment, ancillary facilities and software, but nevertheless this event will mark the opening of new research opportunities. SNS will not replace the science done with neutrons so far at existing sources but rather opens new fields of science for neutrons. A few years after SNS the Japanese J-PARC will start operation, fulfilling partially the demand of the OECD-Megascience Forum from 1998: „*prepare for provision for next generation sources in USA, Europe and Japan*“. It is encouraging to see that the European Spallation Source (ESS) regained some momentum: There are discussions going on in Sweden on the ministerial level, UK is seriously considering its policy concerning the future of neutron sources and there is renewed activity in Germany (Sachsen/Sachsen-Anhalt) and in Hungary towards hosting ESS. For the vast majority of neutron users, it won't matter where ESS will be located as long as it is assured that it will be built somewhere in Europe.

Peter Allenspach

# *Data Reduction on Time-of-Flight Instruments*

*P. L.W. Tregenna-Piggott*

*Laboratory for Neutron Scattering,  
ETHZ and Paul Scherrer Institut,  
5232 Villigen PSI, Switzerland.*

## **1. Introduction**

The conversion of raw neutron-scattering data into physical functions that are, by and large, independent of the instrument is a process known as data reduction. Given that neutron scattering is a mature field, one might be forgiven for thinking that the theory of data reduction is well-established and generally accepted. When joining the Laboratory for Neutron scattering in April of this year, I was therefore somewhat surprised to discover that no such consensus exists for data reduction on the indirect geometry time-of-flight (TOF) instrument, MARS, for which I was to assume responsibility. Coincident with the start of my appointment, there emerged a publication by Bruno Dorner on this very topic.<sup>1</sup> I profess myself to entertain a profound veneration for this work and much of what follows constitutes a summary of his disquisition. I begin by showing how easy it is to follow an erroneous mathematical path that ultimately leads to a set of equations relating raw TOF data to the scattering function, that are intuitively incorrect, for they are asymmetric with respect to the transformation between direct and indirect geometry TOF. I then show how the formalism of Dorner affords a rigorous prescription for data reduction of TOF data that resolves the discrepancy, providing invaluable insight into the physical quantities that are actually being measured.

## **2. Determination of the Scattering Function from TOF Data**

The derivation of how the scattering function may be extracted from a TOF experiment is usually presented as follows. The probability that the infinitesimal flux of neutrons is scattered into the infinitesimal solid angle  $d\Omega_F$  and in the energy window  $dE_F$  is related to the scattering function by,

$$(1) \quad \frac{d^2\sigma}{d\Omega_F dE_F} = \frac{k_F}{k_I} S(Q, \omega)$$

where  $\hbar\omega$  and  $\hbar Q$  are the energy and momentum transfer, and  $k_I$  and  $k_F$  are the incoming and outgoing wavevectors respectively. In equation (1) and in all subsequent equations, all parameters that do not contain spectral components are neglected.

The measured quantity is the intensity of neutrons collected in a given time channel of width  $\Delta\tau$ , confined to the solid angle,  $\Delta\Omega_F$ , which is related to the scattering function  $S(Q, \omega)$  by:

$$(2) \quad I(t) = I_I(t_I, \Omega_I) \Delta\Omega_F p(k_F) \int_0^{\Delta t} \frac{d^2\sigma}{d\Omega_F dE_F} \frac{d\omega}{dt} dt =$$

$$I_I(t_I, \Omega_I) \Delta\Omega_F p(k_F) \frac{k_F}{k_I} \int_0^{\Delta t} S(Q, \omega(t)) \frac{d\omega}{dt} dt$$

where  $I_I(t_I, \Omega_I)$  is the incident neutron flux, and  $p(k_F)$  the detector efficiency.

$\frac{d\omega}{dt}$  may be regarded as a Jacobian needed for the non-linear transformation between time and energy. In a direct TOF experiment, a monochromatic beam of known energy is scattered by the sample;  $t_F$  is the variable whilst  $t_I$  is constant. Equation (2) then becomes,

$$(3) \quad I(t_F) = I_I(t_I, \Omega_I) \frac{k_F}{k_I} \Delta\Omega_F p(k_F) S(Q, \omega(t)) \frac{1}{t_F^3} \Delta t_F \Delta t_I =$$

$$I_I(t_I, \Omega_I) S(Q, \omega(t)) \Delta\Omega_F \Delta t_F \Delta t_I p(k_F) \frac{1}{t_F^4}$$

That the measured intensity, in a given time channel, must be multiplied by a factor of  $t_F^4$  to obtain the scattering function, is a result that is generally accepted for direct TOF geometry. But what is the corresponding procedure for indirect (inverse) TOF geometry? The reader will forgive me for addressing this question in conjunction with a short advertisement for the MARS spectrometer, a schematic for which is shown below:

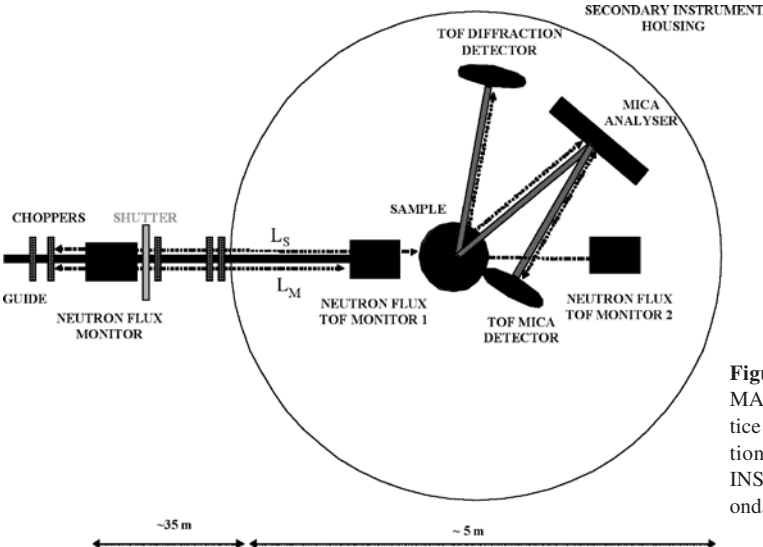


**Figure 1:** Schematic of the MARS Instrument. In practice there are 12 TOF diffraction detectors and 10 TOF INS detectors within the secondary instrument housing.

As the name suggests, the experiment is essentially direct-geometry TOF in reverse. Five choppers located in the primary instrument are used to define a pulse of quasi-white neutrons incident upon the sample. The scattered neutrons that reach the TOF diffraction detectors are employed for the calculation of the Bragg diffraction pattern. The scattered neutrons that reach detectors via the mica analyzer banks are employed for the calculation of the scattering function. The instrument may be configured so that only those neutrons arising from a distinct mica reflection, for example the 002, reach the detector banks. The scattering angle then defines the final energy of the neutrons that may reach the detectors, via Bragg's law.

The MARS spectrometer is unique in offering high-resolution over a wide energy-transfer range, and promises to be a powerful instrument for the study of a wide range of physical phenomena, including translational and rotational diffusion; tunnelling spectroscopy; and, in particular, magnetic excitations, as the design of the spectrometer facilitates the measurement of excitations with large energy transfer with low momentum transfer.

Returning to the topic of discussion, for indirect geometry TOF,  $t_I$  is now the variable whereas  $t_F$  is a constant Equation (2) then becomes,

$$(4) \quad I(t_I) = I_I(t_I, \Omega_I) \frac{k_F}{k_I} \Delta\Omega_F p(k_F) S(Q, \omega(t)) \frac{1}{t_I^3} \Delta t_I \Delta t_F = \\ I_I(t_I, \Omega_I) S(Q, \omega(t)) \Delta\Omega_F \Delta t_I \Delta t_F p(k_F) \frac{1}{t_I^2}$$

We have obtained the rather awkward result that for direct TOF the scattering function and measured intensity are inter-related by a factor of  $t_F^4$ , whereas for indirect TOF the factor is  $t_I^2$ . What have we overlooked? So far we have said nothing about the incoming flux,  $I_I(t_I, \Omega_I)$ . Neutron flux TOF Monitor 1, depicted in Figure 1, is placed upstream from the sample to measure the intensity of the incoming flux. But what exactly does the monitor measure? The question is far from being trivial, and a key achievement of Dorner is to clarify this matter. The following is a summary of his article with a little more explanation and one or two figures thrown in for good measure.

Dorner begins by writing the infinitesimal intensity  $dI$  (counts/sec) collected in a given detector as:

$$(5) \quad dI = dj(k_I) \frac{d^2\sigma}{d\Omega_F dE_F} d\Omega_F dE_F p(k_F) \quad ,$$

where  $dj(k_I)$  is the infinitesimal flux of neutrons incident upon the sample in phase space,

$$(6) \quad dj(k_I) = k_I * p(k_I) dk_{I,x} dk_{I,y} dk_{I,z}$$

The first term on the right-hand side of equation (6) is proportional to the velocity of the neutron, and the second term may be understood as the density of the neutrons in an infinitesimal region of reciprocal space.  $p(k_I)$  is defined by the author as the spectrum of the source. It takes account of the variation in wavelength of the density of the neutrons incident upon the sample. Substituting Equations (1) and (6) into equation (5), we obtain,

$$(7) \quad dI = k_I * p(k_I) dk_{I,x} dk_{I,y} dk_{I,z} \frac{k_F}{k_I} S(Q, \omega) d\Omega_F dE_F p(k_F)$$

Equation (7) may be simplified by writing,

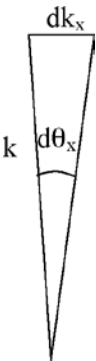
$$(8) \quad dE_F \sim k_F dk_{F,z}$$

and

$$(9) \quad d\Omega_F = \frac{dk_{F,x} dk_{F,y}}{k_F^2}$$

where the z-direction coincides with the direction of  $k_F$ .

Equation (8) follows from  $E = P^2 / 2m$ . Equation (9) may be readily understood by considering the following schematic:

$$(10) \quad \begin{array}{l} \text{dk}_x \\ \text{d}\theta_x \\ \text{k} \end{array} \quad \begin{array}{l} dk_x = k \cdot d\theta_x \\ dk_y = k \cdot d\theta_y \\ d\Omega = d\theta_x d\theta_y = \frac{dk_x dk_y}{k^2} \end{array}$$


Inserting equations (8) and (9) into equation (7) we obtain Dorner's master formula:

$$(11) \quad dI = p(k_I) dk_{I,x} dk_{I,y} dk_{I,z} S(Q, \omega) p(k_F) dk_{F,x} dk_{F,y} dk_{F,z} .$$

Equation (11) is beautiful as it shows that when relating the measured intensity to the scattering function, the incoming beam is symmetric with respect to the scattered beam. Since  $k \sim 1/t$ , equation (11) may be readily converted from phase- to time-space,

$$(12) \quad dI = p(k_I) \frac{1}{t_I^4} d\Omega_I dt_I S(Q, \omega) p(k_F) \frac{1}{t_F^4} d\Omega_F dt_F ,$$

where we have used equation (10) and,

$$(13) \quad dk_z \sim \frac{1}{t^2} dt .$$

Note that the density of neutrons as defined by  $p(k_I) dk_{I,x} dk_{I,y} dk_{I,z}$  is equal to

$$p(k_I) \frac{1}{t_I^4} d\Omega_I dt_I .$$

The measured intensity is obtained by integrating equation (12). Following Dorner we write:

$$(14) \quad S^*(Q, \omega) = \frac{I_{meas}}{V_I V_F} ,$$

where  $S^*(Q, \omega)$  is the scattering function convoluted with the normalised resolution function.

The volume elements are given by,

$$(15) \quad V_I = \int_0^{\Delta\Omega_I \Delta t_I} p(k_I) \frac{1}{t_I^4} d\Omega_I dt_I = p(k_I) \frac{1}{t_I^4} \Delta\Omega_I \Delta t_I ,$$

$$V_F = \int_0^{\Delta\Omega_F \Delta t_F} p(k_F) \frac{1}{t_F^4} d\Omega_F dt_F = p(k_F) \frac{1}{t_F^4} \Delta\Omega_F \Delta t_F .$$

For direct TOF geometry,  $V_I$  is constant, whilst  $V_F$  is a variable. The converse holds for indirect TOF geometry.

At this juncture we are now in a position to resolve the apparent discrepancy between equations (3) and (4). In deriving equation (3), the measured intensity of neutrons scattered from the sample is defined in terms of the flux of neutrons scattered in a given time channel, confined to the solid angle  $\Delta\Omega_F$ . In order for the incoming flux of neutrons to be defined identically, the components of the momenta of the incoming beam perpendicular to  $k_I$ , must be written in terms of the solid angle via. equation (10). By making the following substitution,

$$(16) \quad I_I(t_I, \Omega_I) = p(k_I)k_I^2 \Delta\Omega_I \quad ,$$

equations (3) and (4) are then:

$$(17) \quad I(t_F) = p(k_I)p(k_F)\Delta\Omega_I\Delta\Omega_F\Delta t_I\Delta t_F S(Q, \omega(t)) \frac{1}{t_F^4} \quad ,$$

$$(18) \quad I(t_I) = p(k_I)p(k_F)\Delta\Omega_I\Delta\Omega_F\Delta t_I\Delta t_F S(Q, \omega(t)) \frac{1}{t_I^4} \quad .$$

for direct and indirect TOF geometry respectively, in accordance with equations (14) and (15).

The correction for  $V_I$  may be swallowed up in the counts measured by a monitor positioned before the sample. The intensity measured by the monitor may be written in the general form:

$$(19) \quad I_{monitor} = j(k_I) * E(k_I) \quad ,$$

where  $j(k_I)$  is the incoming neutron flux,

$$(20) \quad j(k_I) = \text{neutron velocity} * \text{neutron density} = k_I V_I$$

and  $E(k_I)$  is the monitor efficiency.

$j(k_I)$  is obtained by dividing the measured monitor counts by  $E(k_I)$ :

$$(21) \quad j(k_I) = \frac{I_{monitor}}{E(k_I)} = I_{black\ det} \quad .$$

$I_{black\ det.}$  is equivalent to measuring the incoming flux with the help of a black detector at the sample position. In practice this may be achieved by measuring the vanadium spectrum with no analyser banks, i.e. using the diffraction detectors depicted in Figure 1.

Dividing the measured intensity by  $I_{black\ det.}$  yields:

$$(22) \quad I_{meas.cor} = \frac{I_{meas}}{I_{black\ det}} = \frac{I_{meas}}{k_I V_I} = S^*(Q, \omega) \frac{V_F}{k_I} \sim S^*(Q, \omega) V_F t_I$$

In short:

$$(23) \quad S^*(Q, \omega) = \frac{I_{meas.cor} k_I}{V_F} \sim \frac{I_{meas.cor}}{t_I V_F}$$

Equation (23) states that if the measured intensity is normalised to the incident neutron flux, then the scattering function is obtained by making the further correction of dividing  $I_{meas.cor}$  by  $t_I$ . The monitor efficiency,  $E(k_I)$ , may be written in the general form,

$$(24) \quad E(k_I) = 1 - \exp(-b\lambda) \quad ,$$

where  $b$  is constant, characteristic of the monitor.

In the instance when  $b\lambda \ll 1$ , equation (24) simplifies to,

$$(25) \quad E(k_I) \approx b\lambda \sim \frac{1}{k_I} \quad .$$

Thus, when the monitor is a weak absorber, we obtain:

$$(26) \quad I_{black\ det.} \sim k_I I_{monitor} = j(k_I) = k_I V_I$$

Hence  $V_I$  is obtained directly,

$$(27) \quad I_{monitor} = V_I \quad .$$

Equation (22) then simplifies to:

$$(28) \quad \frac{I_{meas}}{I_{monitor}} \approx \frac{I_{meas}}{V_I} = S^*(Q, \omega) V_F \quad .$$

The mica 002 reflection corresponds to  $\lambda_f \approx 20 \text{ \AA}$  in backscattering geometry. In principle it should be possible to compare the relative intensities of excitations with  $\lambda_l$  in the range of 1 to 20  $\text{\AA}$ , although it is not possible to cover such a large energy window in one experiment. For the neutron flux monitor 1, on the MARS spectrometer, the constant  $b$  has the value 0.0157, and hence equation (25) is but a fair approximation to the detector efficiency in the 1 to 20  $\text{\AA}$  wavelength range. Thus, the data reduction will be performed directly from equations (21), (23) and (24).

The IRIS instrument, located at ISIS, is an indirect geometry TOF spectrometer, similar in design and concept to MARS, though less versatile. Measurements from this instrument, which has been in operation a number of years, should assist in the experimental verification of the correct data reduction procedure. From information received from the instrument responsible,<sup>2</sup> the conversion of the counts collected *within a given time channel* to the scattering function proceeds in accordance with equation (23). However, it not clear either to me or to Dorner whether the intensity is further multiplied by the factor,

$$(29) \quad \frac{\Delta\lambda}{\Lambda\omega} = \frac{\Delta t}{\Lambda\omega} = \frac{dt}{d\omega} \sim t_f^2 \quad ,$$

where  $\Delta t$  and  $\Delta\omega$  are the widths of the time channels and the corresponding energy channels respectively. The reasoning for including this Jacobian is the non-linear conversion between time and energy. However, as this factor has already been incorporated into the operation of dividing the measured intensity by the monitor counts, the further operation of multiplying the intensity by the factor in equation (29) would not be valid. If the data reduction on IRIS does indeed incorporate this factor, then I believe the data reduction of IRIS data, as presently undertaken, to be incorrect. Compared to a model calculation, experimental data points on the neutron-energy-gain side of the spectrum would be too high in intensity, and data on the neutron energy-loss side too low in intensity.

## 2. Data Reduction and Analysis Software

Recently, a concerted effort has been instigated between neutron-scattering institutions to collaborate on a software package for the interpretation of neutron-scattering data, and I am proud that the PSI is a part of this collaboration. DAVE stands for Data Analysis and Visualisation Environment, and is a series of programs written by Rob Dimeo and his colleagues at the National Institute of Standards and Technology (NIST), Washington D.C., for the reduction and analysis of neutron scattering data. Not only do the NIST team distribute their software freely, they provide introductory courses in Interactive Data Language (IDL) and are more than willing to offer advice and encouragement to scientists from other institutions, wishing to write data reduc-

tion programs within the DAVE environment. FOCUS Data Reduction (FDR) is such a program, and was written by the author of this article, in constant consultation with Fanni Juranyi, presently the person responsible for FOCUS, the direct geometry TOF instrument, here at the PSI. We wanted to conceive a program suitable for the novice as well as the seasoned user, and I believe we achieved this goal. The main interface is shown below.

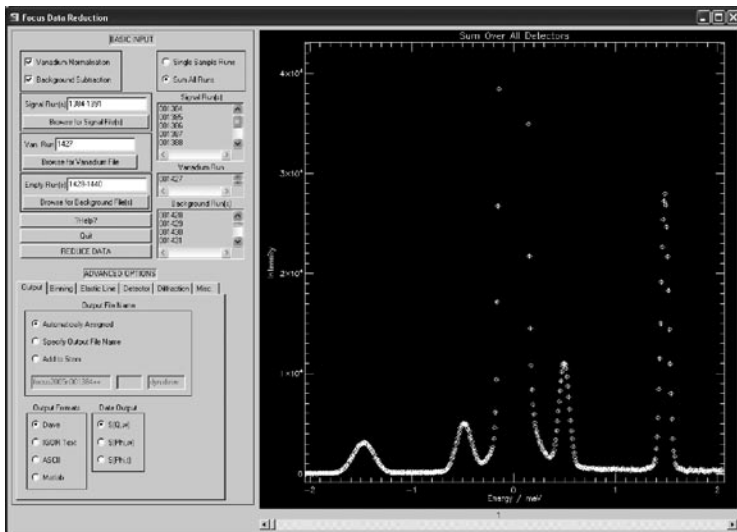


**Figure 2:** Main Interface of the Focus Reduction Program

A minimal amount of input is required to reduce a raw data set; the program chooses sensible defaults for you. On the other hand a sophisticated, user-specific workup of the data may be accomplished using the Advanced Options. Perhaps the most attractive aspect of the program is that subsequent to reduction, the data may be analysed with any one of the excellent programs in the DAVE program suite. We shall now proceed to write the data reduction program for MARS, along with a program to change the variables of the instrument (chopper phases, analyser bank positions etc.) according to scientific specifications, as set out by the user. The motivation for writing good software is clear: the better the software, the less work for the local contact.

## References

- [1] B. Dorner, *Journal of Neutron Research*, vol 13/4 **2005**.
- [2] Felix Fernandez-Alonso, *INS\_Reduction*, private communication.

# *Dynamic Rotational Anion Disorder in Tetrahydroxoborate Sodalite Investigated by Quasielastic Neutron Scattering*

*D. Wilmer, F. Juranyi\*, M. Kalwei, H. Koller*

*University of Münster, Institute of Physical Chemistry and Sonderforschungsbereich 458  
Corrensstr. 30/36, 48149 Münster, Germany*

*\*Laboratory for Neutron Scattering, Paul Scherrer Institut,  
5232 Villigen PSI, Switzerland*

## **Abstract**

The dynamic rotational disorder of tetrahydroxoborate anions,  $\text{B}(\text{OH})_4^-$ , in tetrahydroxoborate sodalite,  $\text{Na}_8[\text{AlSiO}_4]_6[\text{B}(\text{OH})_4]_2$ , has been investigated in several quasielastic neutron scattering experiments using the time-of-flight spectrometer FOCUS. Above a phase transition at about 303 K, the complete anion unit reorients, probably by jump diffusion, with residence times between 100 ps (310 K) and 3 ps (420 K), the reorientation rates being activated with 0.14 eV. There is evidence for an additional faster proton motion restricted to a circle around a B-O bond. Accompanying measurements of the ionic conductivity show that the sodium ions, although identified as locally mobile in an earlier NMR investigation, exhibit moderate long-range transport properties only. Possible dynamic correlations between the localized motions of hydroxoborate anions and sodium cations obviously do not lead to an enhanced sodium ion conductivity.

## **Introduction**

Zeolites are crystalline porous aluminosilicates which contain charge balancing cations in their extra-framework voids. The cation concentration depends on the charge density of the aluminosilicate framework, i.e., the number of Al atoms in tetrahedral position per unit cell.

In spite of the high concentration of extra-framework cations, the ionic conductivities of zeolite systems reported so far are relatively poor, evidently due to the low cation mobility. In this paper, we report on our investigations of tetrahydroxoborate sodalite, a material which was regarded as a potential sodium conductor.

The sodalite framework consists of space-filling  $4^6 6^8$  (sodalite) cages with alternating  $\text{AlO}_{4/2}^-$  and  $\text{SiO}_{4/2}$  tetrahedra. Figure 1 shows a wire model of the sodalite cage where the corners represent Si and Al centres and the framework oxygen atoms are omitted.

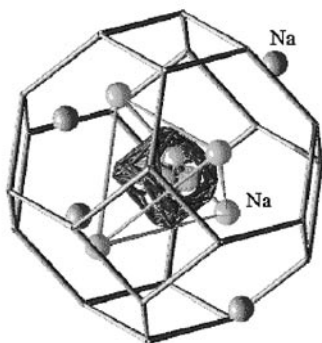


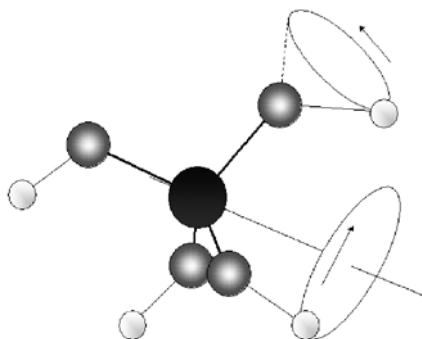
**Figure 1:** Sodalite cage with four tetrahedrally arranged sodium ions inside and outside the cage of tetrahydroxoborate sodalite. The  $\text{B(OH)}_4^-$  anion resides close to the center of the cage; the representation in the figure emphasises its orientational disorder.

In tetrahydroxoborate sodalite, each cage contains four sodium atoms at positions close to the sodalite cage six-rings in a tetrahedral arrangement and an orientationally disordered  $\text{B(OH)}_4^-$  anion [1]. In a static picture, sodium atoms in neighboring sodalite cages are located at the opposite side of those six-rings which are not “blocked” by sodium atoms inside the cage. At 303 K, the material exhibits a phase transition induced by the onset of dynamical processes [2]. The high-temperature phase is cubic with  $a=9.015\text{\AA}$ , the space group is  $P43n$ . Above the phase transition temperature,  $^{23}\text{Na}$ -NMR-MAS spectra show considerable line narrowing and a single sodium position, indicating an enhanced sodium ion mobility [3]. The detailed analysis of  $^{11}\text{B}\{^1\text{H}\}$  and  $^{11}\text{B}\{^{23}\text{Na}\}$  NMR-REDOR measurements performed at 320 K suggests that on the NMR time scale, the  $\text{B(OH)}_4^-$  anions undergo isotropic reorientations while the sodium ions exhibit a restricted, non-isotropic dynamics [3]. A key question here is whether and to what extent the reorientation of the hydroxoborate anions enhances the cation mobility in the sense of what has become famous under the term *paddle-wheel mechanism* [4].

At 260 K, i.e., below the phase transition temperature, the NMR results agreed well with the predictions of a model which considers a rotation of protons around all B-O bonds as well as a rotation of the whole  $\text{B(OH)}_4^-$  unit around one B-O bond, cf. Fig. 2.

The NMR results could neither give the anion reorientation rates nor could they characterise the long range cation transport. We, therefore, decided to perform a quasi-elastic neutron scattering study to reveal further details of the anion reorientation motion, accompanied by conductivity measurements to investigate the cation conduc-

**Figure 2:** Sketch of the hydroxoborate anion,  $\text{B(OH)}_4^-$ . The  $\text{BO}_4$  unit forms a regular tetrahedron with a B-O bond length of  $1.477\text{\AA}$ . The O-H bond length is assumed to be  $0.91\text{\AA}$ , the B-O-H bond angle close to  $161^\circ$ , in analogy to borate hydrates [5]. The sketch shows a conceivable type of anion reorientation, i.e., a combination of proton rotation on a circle around a fixed B-O axis and rotation of the whole unit, here shown to take place around one of the tetrahedral  $\text{C}_3$  axis. The predictions of this dynamic model proved to be in good agreement with the NMR-REDOR data measured at 260 K, i.e., in the low-temperature phase.



tivity. Since protons are moving during reorientation of the  $\text{B}(\text{OH})_4^-$  units and the dynamic neutron scattering behaviour is dominated by the protons' large incoherent scattering cross section, quasielastic neutron spectroscopy is ideally suited to investigate hydroxoborate reorientation in our system.

## Experimental

Samples of  $^{11}\text{B}$ -enriched tetrahydroxoborate sodalite were prepared by hydrothermal synthesis. Details on the synthesis may be found elsewhere [3]. The use of  $^{11}\text{B}$ -enriched samples reduces neutron loss due to the high neutron absorption cross section of  $^{10}\text{B}$ . The powder samples are neither hygroscopic nor otherwise sensitive and thus easy to handle. For the neutron scattering experiments, samples were filled into indium-sealed, cylindrical thin-walled (0.5 mm) aluminium cans (10 mm diameter, 50 mm length) available at the spectrometer. Sample masses for the two sets of neutron scattering experiments were 2.7 g and 3.3 g.

Quasi-elastic neutron scattering spectra were collected on the time-of-flight spectrometer FOCUS, located at the Paul-Scherrer-Institute, Villigen, Switzerland. Data were collected at four temperatures above the 303 K phase transition but well below decomposition which commences above 450 K with a loss of water and ends in a collapsing lattice at even higher temperatures.

In a first set of experiments, FOCUS was operated in the time-focussing mode using the PG002 monochromator. Using two different take-off angles offered the opportunity to select two incident neutron wavelengths and elastic energy resolutions. In a second set of experiments, we used the relatively new mica monochromator (002 reflexion) to obtain even better resolution (22  $\mu\text{eV}$  FWHM) at the expense of neutron flux and scattering vector range. Table 1 summarises the parameters of the neutron scattering experiments on FOCUS.

Wavelength/ $\text{\AA}$	4.3	5.7	11.8
$Q_{\text{max}}/\text{\AA}^{-1}$	2.7	2.0	0.99
Resolution/ $\mu\text{eV}$ FWHM	140	52	22

**Table 1:** FOCUS instrument parameters for the measurements on tetrahydroxoborate sodalite. The experiments at 4.3  $\text{\AA}$  and 5.7  $\text{\AA}$  used the PG002 monochromator; MICA002 offered the highest resolution setup.

The time-of-flight data were normalized and corrected for detector sensitivity using scattering data of a vanadium sample, regrouped and converted to the energy transfer scale using the FOCUS standard package for raw data treatment, NATHAN.

Additional conductivity measurements to investigate sodium ion transport properties in our sodalite system used uniaxially pressed (10 kbar) cylindrical samples of

$\text{Na}_8[\text{AlSiO}_4]_6[\text{B}(\text{OH})_4]_2$  whose circular faces were sputter-coated by thin gold layers which served as electrodes. Measurements used a Novocontrol Alpha high resolution dielectric analyser in a frequency range from 0.1 Hz to 3 MHz.

## Results and Discussion

The first measurements (PG002 monochromator) with elastic energy resolutions of 52  $\mu\text{eV}$  and 140  $\mu\text{eV}$  FWHM revealed quasielastic broadening at all temperatures (310 K to 420 K) above the phase transition. In a first phenomenological data analysis, a simple model featuring a single Lorentzian plus an elastic contribution, both convoluted with the instrument resolution function, was fitted to all spectra. The resulting elastic-incoherent structure factor (EISF) strongly depended on temperature and resolution. At constant temperature, the line widths do not depend much on the scattering vector modulus  $Q$ , indicating that, in accordance with our expectations, we are monitoring a rather localized type of motion. The detected EISF tendency to decrease with increasing resolution and increasing temperature indicated that the reorientation of the anions was too slow to be fully resolved at the given instrumental setups. A simple solution to this problem, i.e., an increase in temperature to accelerate the reorientation, would fail due to the decomposition of the sample. We, therefore, decided to use the relatively new MICA monochromator option [6] on FOCUS to obtain higher resolved quasielastic spectra. An example spectrum with a resolution of 22  $\mu\text{eV}$  FWHM is given in Figure 3.

The spectra obtained from the MICA setup could easily be fitted using a single Lorentzian plus an elastic contribution, both broadened with the elastic energy resolution function, cf. Figure 3. Simultaneous fitting of all spectra (five different  $Q$  values) measured at the same temperature yielded, for the first time, characteristic residence

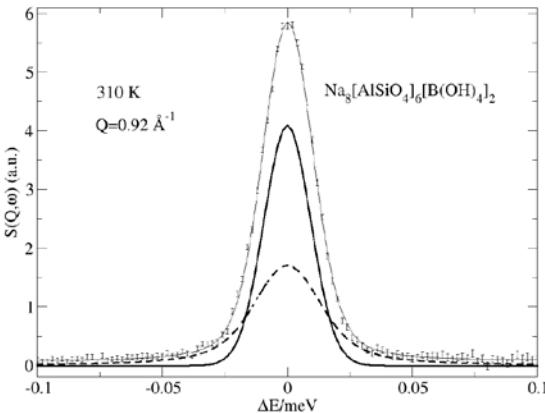


**Figure 3:** Example spectrum of tetrahydroxoborate sodalite,  $\text{Na}_8[\text{AlSiO}_4]_6[\text{B}(\text{OH})_4]_2$ , measured on FOCUS using the MICA monochromator [6]. Error bars symbolise measured data. Thin solid line: fit using an elastic component (thick solid line) and a quasielastically broadened Lorentzian (dashed line), both broadened by the elastic resolution function.

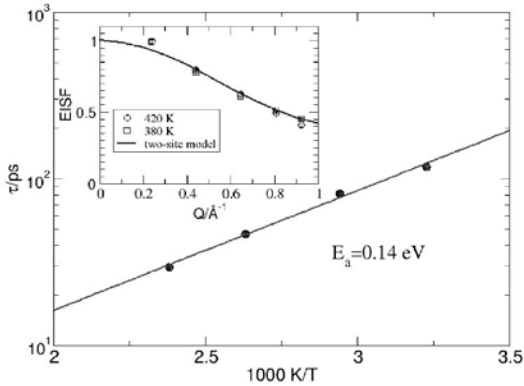


**Figure 4:** Characteristic residence times and elastic-incoherent structure factor of tetrahydroxoborate sodalite,  $\text{Na}_8[\text{AlSiO}_4]_6[\text{B}(\text{OH})_4]_2$ , measured at  $22 \mu\text{eV}$  resolution (MICA setup).

times for the anion reorientation which range from 3 ps (420 K) to about 100 ps (310 K) and exhibit an Arrhenius-type temperature dependence, cf. Figure 4. The activation energy is 0.14 eV. Moreover, we now obtain an EISF which no longer depends on temperature, i.e., we now seem to fully resolve the quasielastic broadening due to the hydroxoborate reorientation.

Unfortunately, the high-resolution MICA setup caused an incident neutron wavelength of  $11.8 \text{ \AA}$ , resulting in a rather limited  $Q$  range with a maximum of about  $1 \text{ \AA}^{-1}$ . An analysis of the spatial details of the anion reorientation based on the EISF is thus not feasible, i.e., it is hardly possible to decide whether we observe isotropic rotational diffusion or whether the protons perform a more restricted type of motion, e.g., jump diffusion around one of the tetrahedral symmetry axes.

The observed EISF indicates, however, a reorientation of the whole  $\text{B}(\text{OH})_4^-$  unit – rotation of the proton around a single B-O axis would only lead to a slight decrease of the EISF in the given  $Q$  range.

Further spatial details will be obtained from a recently performed quasielastic experiment on the backscattering spectrometer IRIS (ISIS, Didcot, UK) which offers a unique combination of high resolution and large  $Q$  range. Details will be reported elsewhere, as soon as the data are fully analyzed.

On the basis of the spectra obtained using the MICA setup, it is possible to improve the data analysis of our initial PG002 measurements: we now perform a simultaneous fit to all spectra obtained at a given temperature with a model which uses *two* quasielastic components plus an elastic part. In these fits, we constrain the Lorentzian line widths for all  $Q$  values to a single value but let their weights vary. In addition, we fix the line width of the smaller component to the value obtained from the analysis of the MICA measurements. Under these conditions, we obtain the quasielastic intensities (at 420 K) shown in Figure 5. For comparison we present the results of a calculation

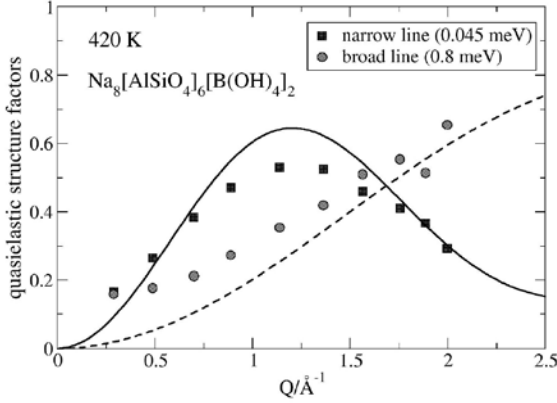


**Figure 5:** Quasielastic intensities (filled symbols) of  $\text{Na}_8[\text{AlSiO}_4]_6[\text{B}(\text{OH})_4]_2$ , extracted from the  $5.7 \text{ \AA}$  data (PG002 setup,  $52 \text{ \mu eV}$  FWHM elastic energy resolution). Solid and dashed lines are results of our model calculation.

based on a model which considers both jump diffusion of the whole anion unit around the spatially fixed  $C_2$  and  $C_3$  axis and jump diffusion of the protons around the (mobile) B-O axes [7].

It is obvious that the general characteristics of the measured quasielastic intensities are reasonably well represented by the model curves. The narrower quasielastic component which essentially reflects the (slower) reorientation of the whole  $\text{B}(\text{OH})_4^-$  unit exhibits its intensity maximum at  $Q \approx 1.2 \text{ \AA}^{-1}$ ; due to its reduced radius, the faster proton rotation around the B-O axes causes a quasielastic intensity with smaller slope when plotted against the scattering vector  $Q$ . It is interesting to note that the scenario found here by quasielastic neutron scattering *for the high-temperature phase* agrees well with the result of the NMR measurements *for the low-temperature phase*. No reasonable fits to the quasielastic high-temperature phase spectra could be obtained using the isotropic diffusion model [8] although the NMR investigations gave a clear

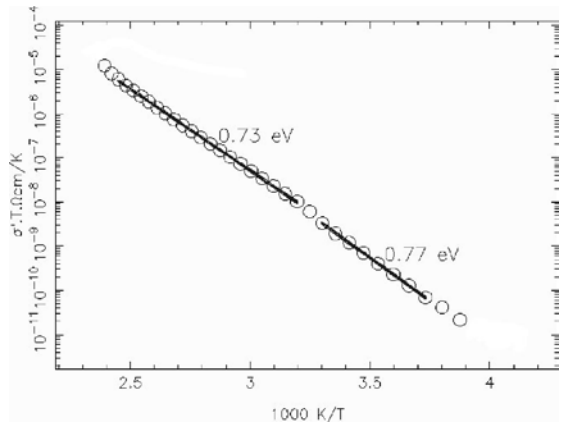


**Figure 6:** Total electrical conductivity of  $\text{Na}_8[\text{AlSiO}_4]_6[\text{B}(\text{OH})_4]_2$  as a function of temperature (Arrhenius representation).

indication for the isotropic reorientation of the hydroxoborate anion [3]. This is probably due to the fact that neutron time-of-flight spectroscopy is sensitive to a much shorter time scale than NMR measurements.

Our conductivity measurements on tetrahydroxoborate sodalite show that the high sodium ion mobility detected in the NMR measurements [3] is indeed of localized nature. The Arrhenius representation of our dc conductivity data (cf. Figure 6) shows that tetrahydroxoborate sodalite, in spite of its local cation mobility, is only a moderate sodium ion conductor, i.e., its local mobility does not transform into a considerable long-range ion transport. Activation energies found here are significantly higher (0.73 eV and 0.77 eV above and below the phase transition temperature, respectively) than for the anion reorientation, and there is hardly any change of slope at the phase transition temperature.

We, therefore, have to conclude that in tetrahydroxoborate sodalite, we cannot detect a dynamic correlation between the dynamic rotational disorder of the anions and the long range transport of the cations. Nevertheless, there might well be a close correlation between the  $B(OH)_4^-$  reorientation and the local sodium motion inside the sodalite cage.

## Acknowledgement

Experiments reported in this work were partially performed at the spallation neutron source SINQ, Paul-Scherrer-Institut, Villigen, Switzerland. Financial support by the German Federal Ministry of Education and Research and by the German Science Foundation (DFG, SFB 458) is gratefully acknowledged.

## References

- [1] J. C. Buhl, C. Mundus, J. Löns, W. Hoffmann, *Z. Naturforsch.* 49a (1994) 1171.
- [2] G. Engelhardt, P. Sieger, J. Felsche, *Analytica Chimica Acta* 283 (1993) 967.
- [3] H. Koller, M. Kalwei, *J. Phys. Chem. B.* 108 (2004) 58.
- [4] A. Lundén, *Solid State Ionics* 28-30 (1988) 163; *Solid State Comm.* 65 (1988) 1237.
- [5] C.C. Freyhardt, in „Bildung und Charakterisierung kristalliner Phasen in Systemen  $(NR_4)O \cdot B_2O_3 \cdot H_2O$ “, Hartung-Gorre-Verlag, Konstanz 1996.
- [6] F. Juranyi, S. Janssen, J. Mesot, L. Holitzner, C. Kägi, R. Tuth, R. Bürge, M. Christensen, D. Wilmer, R. Hempelmann, *Chem. Phys.* 292 (2003) 495.
- [7] M. Bée, *Quasielastic Neutron Scattering*, Adam Hilger, Bristol 1988.
- [8] V. F. Sears, *Can. J. Phys.* 45 (1967) 234.

# *ICON – The New Facility for Cold Neutron Imaging at the Swiss Spallation Neutron Source SINQ*

*G. Kühne<sup>1</sup>, G. Frei<sup>1</sup>, E. Lehmann<sup>1</sup>, P. Vontobel<sup>1</sup>,  
A. Bollhalder<sup>2</sup>, U. Filges<sup>2</sup>, M. Schild<sup>2</sup>*

*<sup>1</sup> Neutron Imaging and Activation Group (NIAG), ASQ Division*

*<sup>2</sup> Laboratory for Developments and Methods (LDM)*

*Paul Scherrer Institut, 5232 Villigen PSI, Switzerland*

## **Abstract**

Based on the very good experience and knowledge gained with thermal neutron radiography at NEUTRA, novel capabilities can be predicted for the new beam-line with cold neutrons: Micro tomography, neutron phase contrast imaging, contrast enhanced radiography, improved quantification of tracer elements and energy selective neutron imaging.

The two main conditions for high quality neutron imaging – radiography, tomography and especially for neutron phase contrast imaging – are a high beam collimation and a sufficiently high neutron flux. It was examined whether neutron guides in the accessible parts of the beam channel for ICON could enhance the performance of the instrument. The following findings resulted: 1) the enhanced divergence provided by the guide is not matched to the collimation (L/D ratio) planned for the instrument and 2) the extended image size provided by the guide is not homogeneously illuminated. It has therefore been decided not to use guides inside the target block.

The new radiography beam line ICON for imaging with cold neutrons is installed at channel 52 of the spallation neutron source SINQ. It has a direct view onto the liquid deuterium cold source. There are two standard experiment positions at different distances L from the beam port exit and five different aperture sizes D in the diaphragm system can be chosen.

Different beam characterisation measurements have been done. The neutron spectrum was acquired with the TOF-technique. The accordance with the calculation was quite good for wavelengths greater than 1 Ångstrom. The maximum flux density at the beam port exit with an aperture size of 8 cm was determined with Gold foil activation. Beam sizes and profiles at the two main experiment positions have been analyzed using imaging plates. The neutron and gamma dose measurements have been performed in collaboration with the radiation protection group.

The inauguration of ICON was celebrated during the International Workshop on “Neutron Imaging using Cold Neutrons” held on October 13th and 14th 2005 at PSI.

The first four long-term experiments (duration more than one week) will be finished until end of this year.

## 1. Introduction

The first steps in neutron radiography at the Paul Scherrer Institute (PSI) were made in the late 80’s of the last century at the swimming pool research reactor SAPHIR. The final shutdown of the reactor at the end of 1993 imposed a temporary stop to neutron radiography at PSI. A new neutron radiography facility (NEUTRA) [1] was designed for the spallation source SINQ. Together with the operational start of SINQ at the end of 1996, the first tests concerning beam properties and new detector systems could be performed. The last seven years of NEUTRA show a successful story of development. The progress is two-fold: One in imaging techniques, detector and camera systems and the other in an increasing number of internal and external users from universities and industries [2, 3, 4].

ICON – the new neutron imaging facility with cold neutrons is now an ideal extension to NEUTRA.

## 2. Background

The advantage of cold neutrons for imaging purposes is their higher contrasts for most of the sample materials and the higher detection probability. Therefore, thinner detectors can be utilized and higher spatial resolution achieved as a consequence. Tomography investigations (so called micro-tomography) are planned with the goal to approach the 30  $\mu\text{m}$  resolution range never reached before for digital neutron tomography.

Equipped with an energy-selecting device, narrow energy bands can be cut out from the cold spectrum in those regions where the Bragg edges are located. This will enable the enhancement of contrasts for specific materials.

Two approaches in phase contrast imaging are under consideration: phase contrast imaging with the pinhole geometry for edge enhancement is well suited for cold neutrons, since the phase shift is proportional to the neutron wavelength. And secondly: First experiments on differential phase contrast imaging using a grating interferometer gave already some promising results.

The main prerequisites for high quality neutron imaging in radiography, tomography and especially in neutron phase contrast imaging are high beam collimation, high flux,

and low background. The compliance of these conditions requires a compromise to be made between resolution and intensity. In order to extract as many neutrons as possible from the given cold source, the use of a neutron guide is often essential. The neutron guide transports neutrons of long wavelengths (slow or cold neutrons) by total reflection up to an angle of  $0.1^\circ$  per Ångström of neutron wavelength. For radiography, this inherent divergence of the neutron beam makes it difficult to obtain sharp images, for which a parallel beam is needed. The sharpness of an image is directly dependent on the L/D ratio. D is the diaphragm diameter and L is the flight path length, i.e., the distance from the diaphragm to the detector. An increase of the L/D ratio, in order to obtain a sharper image by closing the diaphragm (decreasing D) or by increasing the distance to the detector L, has the consequence of a decrease in neutron flux and therefore a longer exposure time. The effect of a neutron guide in the inner part of the beam plug has been investigated by Monte Carlo simulation. For the simulation of the relevant neutron data (wavelength distribution, neutron flux, two dimensional spatial distribution of the neutrons at different positions of the beam path), the software package McStas version 1.7 [5] was used. The much better homogeneity of the two-dimensional neutron distribution for the layout without neutron guide was – despite a decrease of neutron flux by a factor three – the reason to keep away from neutron guides in the design.

The comfortable space and infrastructure will enable complementary experimental conditions to the already existing thermal neutron radiography station NEUTRA.

### 3. Experimental setup

#### 3.1 Experimental area

The experimental area (fig. 1) is a concrete construction (bunker), which contains the whole experiment setup. It is controlled by an admission safety system, the Local Access Control (LAC) system.

The first two meters up-beam in the bunker (Nr. 1 in fig. 1) are separated from the rest by concrete shielding blocks and a closed door, also controlled by the safety interlock system LAC. In this inner bunker, activated components like the fail-safe shutter, the experiment shutter, the velocity selector, the time-of-flight chopper and the Beryllium filter and other equipment can be placed. In experiments where no additional components are necessary, an evacuated flight tube is mounted.

A horizontally movable *fail-safe shutter* is placed directly at the beam port exit. It is a sandwich construction consisting of 10 cm thick borated (5 %) Polyethylene, 0.5 mm Gadolinium and 1 cm Lead. The closing time is less than two seconds. A pressure storage tank, whose nominal value is controlled, guarantees the fail-safe condition.

Behind the fail-safe shutter, a fast *experiment shutter* (closing time: 100 ms; composition: 2 mm  $^6\text{LiF}$  and 5.5 mm  $\text{B}_4\text{C}$ ) is positioned.

The design of the ICON facility is versatile: Two measuring positions for experiments and enough space for additional user equipments are available. The position 2 is suited for smaller objects and can be equipped with the micro-tomography and scanning table, whereas at the position 3 large and heavy (up to 500 kg) objects with high collimation can be imaged.

Two *beam limiters* (motorized diaphragms) are available: one in a fixed position inside the inner bunker and the other in front of the respectively probe position 2 or 3.

Behind position 3, a neutron and gamma absorbing *beam dump* is placed. The  $\gamma$ - and n-dose measurements have shown, that the shielding isn't sufficient for the two large aperture openings. During the next shut-down period the shielding back plane has to be improved.

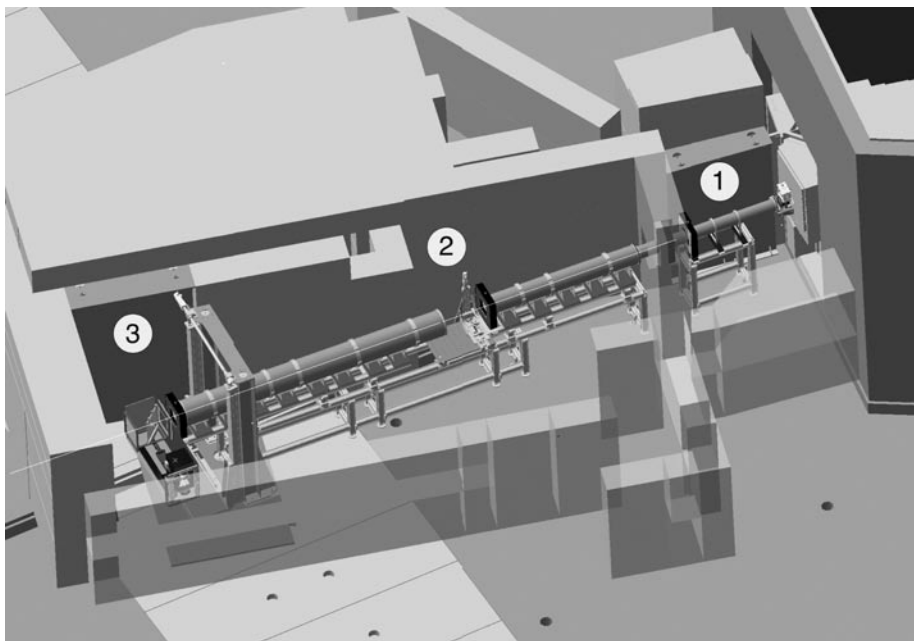


**Figure 1:** Inside the ICON bunker: Nr. 1 shows the inner bunker, where a velocity selector, filters and other equipments can be inserted into the flight path of neutrons. Nr. 2 and 3 are the standard experimental positions. At the position Nr. 2 small and light probes can be examined (e.g. micro-tomography), where at position Nr. 3 bigger and heavier probes can be scanned through the neutron beam.

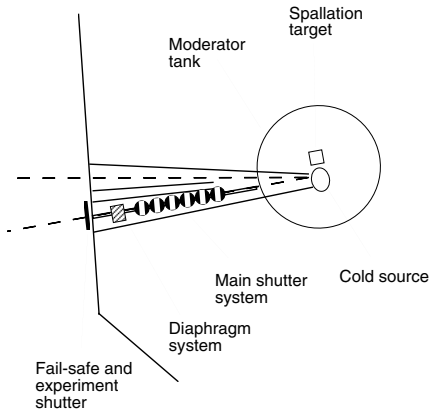


**Figure 2:** Simplified cross section of SINQ with the spallation target, the cold source and the inner collimator containing the main shutter system and the diaphragm system.

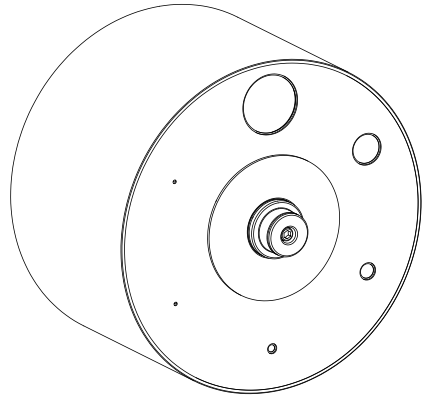


**Figure 3:** Turnable diaphragm system with six different apertures (8 cm, 4 cm, 2 cm, 1 cm, 0.1 cm and 0.05 cm) seen from the neutron entrance side. The length of the diaphragm system is 30 cm.

### 3.2 The inner collimator

The target block inserts placed in the beam channel contain the inner collimator (fig. 2). In the helium gas filled insert the cold neutrons are extracted from the cold source to the front end of the collimator which has a square opening of 8 cm x 8 cm. This collimator opening is surrounded by iron shielding throughout the whole length of the inner collimator (total length 4.4 m).

The central part of the collimator is equipped with six revolving drums, which are used as a shutter to switch off the beam. The first and the last half drum are filled with boron carbide to increase the shielding performance of the shutter against low energy neutrons (thermal and cold neutrons). The other four drums are made of steel in order to shield high-energy neutrons and gamma rays.

In the last part of the inner collimator (just after the revolving drums), a turnable diaphragm system (Fig. 3) is situated. The diaphragm system is made of steel and has a length of 30 cm. The neutron entrance side is covered with 1 mm thick Gadolinium plates in which the apertures have been machined. The six apertures ( $D = 8$  cm, 4 cm, 2 cm, 1 cm, 0.1 cm and 0.05 cm) can be chosen depending on the required L/D ratio (range see tables 2 and 3) or for phase contrast imaging.

All free space around the components inside the target is filled with a helium atmosphere to avoid the activation of air. At the exit of the target block, there is a helium-tight Aluminium window, which can be penetrated easily by the collimated neutron beam.

## 4. Beam Characterisation – Results

### 4.1 Beam sizes

The measured values of the homogenous flat region (plateausize) in the beam profiles in horizontal and vertical direction for all apertures are given in the following tables for the two experiment positions [6].

Position 2: L = 7.10 m from aperture D			
D [cm]	L/D	Plateau-size	
		horiz.	vert.
8	89	—	—
4	178	3 cm	7 cm
2	355	4 cm	7 cm
1	710	8 cm	13 cm
0.1	7'100	8 cm	18 cm
0.05	14'200	8 cm	18 cm

**Table 1:** Beam sizes at position 2

Position 3: L = 12.10 m from aperture D			
D [cm]	L/D	Plateau-size	
		horiz.	vert.
8	151	—	—
4	303	8 cm	7 cm
2	605	15 cm	23 cm
1	1210	16 cm	28 cm
0.1	12100	13 cm	32 cm
0.05	24'200	12 cm	31 cm

**Table 2:** Beam sizes at position 3

The calculated  $L/D$ -expression indicates the collimation of the beam, which is a measure for the neutron image quality (e.g. sharpness). The sharpness of the image increases with the  $L/D$  value, while the neutron flux (number of neutrons which arrive the probe and the detector) decreases. Therefore a compromise between image quality and measuring time (and possible probe activation) has to be found for each experiment.

A neutron image of the open beam at position 2 with an aperture of 2 cm is shown in figure 4 and the corresponding profiles in figure 5.

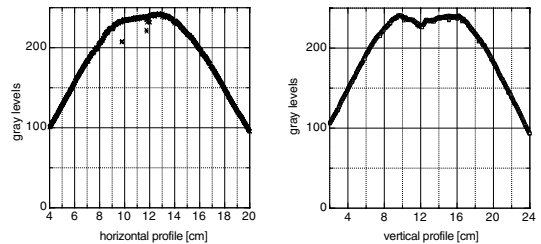


**Figure 5:** Horizontal (left) and vertical (right) profile of the image in figure 4.

**Figure 4:** Open beam image at position 2 and aperture size 2 cm.

## 4.2 Neutron spectrum and flux

The neutron spectrum was measured using the Time-Of-Flight technique with a B<sub>4</sub>C-steel chopper (Jülich-Chopper). The comparison with the calculated spectrum (see fig. 6) shows a discrepancy for wavelengths shorter than about 1 Å. The cold neutron source used in the McStas simulation is a three temperature Maxwell distribution, which is a correct assumption for beam lines with neutron guides which cut off the shorter wavelengths of the non-moderated high-energy spallation neutrons. In the ICON beam line this is not the case; the short-wavelength neutrons appear in the beam.

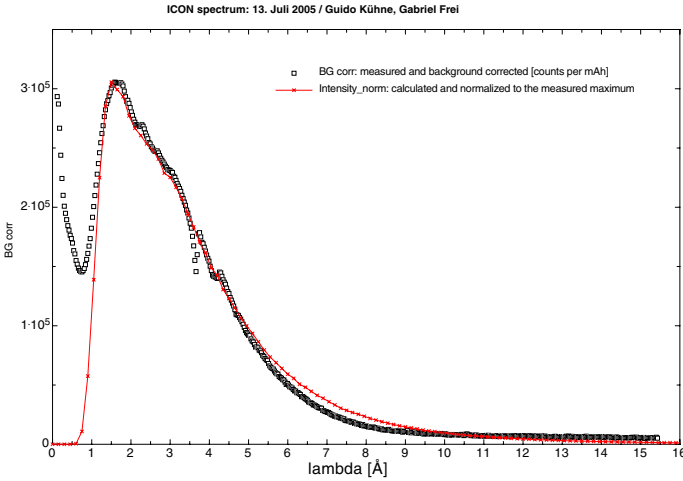


**Figure 6:** Comparison of the measured (black squares) and the calculated (line) wave-length spectrum.

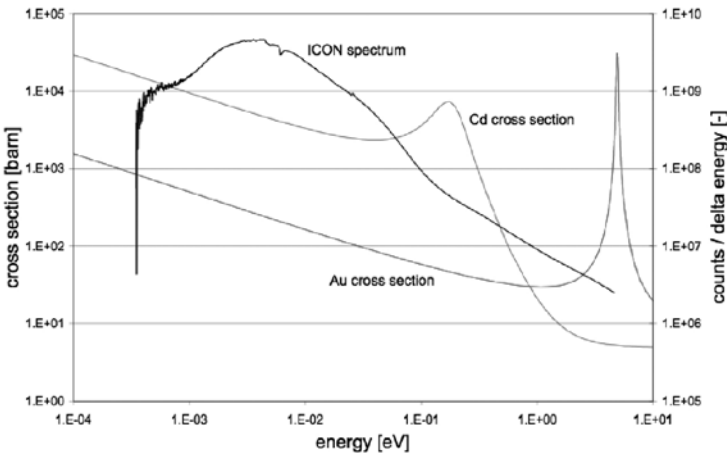


**Figure 7:** Energy spectrum and the cross sections of Gold and Cadmium.

The neutron flux was determined by the gold foil activation technique. Different Gold foils with and without a Cadmium shielding have been activated at the beam port exit with an aperture size of 8 cm. For the evaluation the TOF measurements, cross-sections of Au and Cd (see fig. 7) have been used for the energy weighing of the cross sections [6]. The corresponding results are summarized in table 3.

Energy range	Neutron flux density		
0 ... 10 eV	$4.5 \cdot 10^8 \text{ cm}^{-2} \cdot \text{s}^{-1}$	100 %	total
0 ... 1 eV	$4.3 \cdot 10^8 \text{ cm}^{-2} \cdot \text{s}^{-1}$	96 %	cold / thermal
1 ... 10 eV	$1.9 \cdot 10^7 \text{ cm}^{-2} \cdot \text{s}^{-1}$	4 %	epithermal

**Table 3:** Measured neutron flux density at beam port exit and aperture 8 cm

### 4.3 Neutron dosimetry and shielding

The neutron dose measurements [7] behind the back plane resulted in a too high value for the two large aperture sizes (8 cm and 4 cm). Therefore these openings cannot be used until the shielding of the back plane is optimized. The corresponding Monte-Carlo calculations are on the way. The first results have been validated with repeated neutron dose measurements. The reason for the insufficient shielding effectiveness of the existing back plane was an underestimation of the fraction of high-energy spallation neutrons in the ICON cold beam. The neutron dose measurements have been performed with the standard PSI neutron dose rate meters (ICRU-spheres), which can indicate dose rates for neutrons with energies below 20 MeV. To determine the flux of very high-energy neutrons ( $E > 20 \text{ MeV}$ ), the so-called C-11 measurement was realized [8]. The irradiation of a  $^{12}\text{C}$  containing crystal sample with high-energy neutrons can be described with the following reaction equation:  $^{12}\text{C} + n_{\text{fast}} \rightarrow ^{13}\text{C} \rightarrow ^{11}\text{C} + 2n$ . With the positron-decay of  $^{11}\text{C}$  the very high-energy neutron flux was determined to  $1.1 \cdot 10^5 \text{ cm}^{-2} \cdot \text{s}^{-1}$ . According to the already mentioned Monte-Carlo calculations the very high-energy neutrons give a non-negligible contribution to the neutron dose rate, which cannot be indicated by the standard PSI neutron dose rate meters. Therefore and because of the planned boost of the proton current in the future, the construction of the new shielding has to be conservative.

## 5. Detectors and camera systems

Neutron radiography images will be recorded by a high performance 2048 x 2048 pixel CCD camera system Andor DV 436 from Andor Technology, looking on to a  $^6\text{Li}$  based neutron scintillator screen, which has been optimized in performance and price in our group. The camera and a custom-made lens optic system (1:1 optic) will be mounted

on a common bench. One of our goals is the improvement of the spatial resolution. With this camera we have a nominal pixel size of  $13.5\ \mu\text{m}$  (CCD chip size:  $2.76\ \text{cm} \times 2.76\ \text{cm}$  and  $2048 \times 2048$  pixels). If the producer of the 1:1 optic can fulfil the specifications as offered we believe to reach at least a resolution of  $30\ \mu\text{m}$ .

For dynamic neutron radiography, imaging with either an intensified CCD camera system or an amorphous Silicon based flat panel will be used. Static radiography with the inherently highest possible resolution will be performed with the imaging plate technique (BAS-2500:  $40\ \text{cm} \times 20\ \text{cm}$  / pixel size:  $50\ \mu\text{m}$  and VistaScan:  $10\ \text{cm} \times 10\ \text{cm}$  / pixel size:  $12.5\ \mu\text{m}$ ). Some promising other imaging techniques based on CMOS technology or pixel detectors (e.g. PILATUS-N, a PSI development) are under consideration too.

In this way, a high flexibility and optimal performance is guaranteed for cold neutron imaging in as many applications as possible.

## 6. Outlook

Beside the usual external and internal user program the main topics for further investigations are energy selective imaging either using a neutron chopper and a triggered camera or using a velocity selector and phase contrast imaging with either a pinhole geometry or a grating interferometer technique.

## Acknowledgments

We would like to thank all the PSI staff that has been involved in this project for professional excellence and enthusiasm, in particular those from the PSI workshop, the Neutron Spallation Source division ASQ and last but not least to Kurt Clausen, the head of our department for critical and helpful discussion.

## References

- [1] E. Lehmann et al., Nucl. Instr. and Meth. in Phys. Res. A 377 (1996) 11–15
- [2] B. Winkler, K. Knorr, A. Kahle, P. Vontobel, E. Lehmann, B. Hennion, G. Bayon: Neutron imaging an neutron tomography as non destructive tools to study bulk-rock samples, European Journal of Mineralogy, Vol 14, 2002
- [3] E. Lehmann, P. Vontobel, A. Herrmann: Non-destructive analysis of nuclear fuel by means of thermal and cold neutrons, Nucl. Instr. and Meth. in Phys. Res. A 515 (2003) 745–759

- [4] D. Goers, M. Holzapfel, W. Scheifele, E. Lehmann, P. Vontobel, P. Novak: In situ neutron radiography of lithiumion batteries: the gas evolution on graphite electrodes during the charging, *Journal of Power Sources*, 130 (2004) 221–226
- [5] P. Willendrup, E. Farhi, K. Lefmann, P.-O. Åstrand, M. Hagen and K. Nielsen: User and Programmers Guide to the Neutron Ray-Tracing Package McStas, Version 1.7, Risø-R-1416(EN), Risø National Laboratory, Roskilde, Denmark, May 2003
- [6] E. Meier, R. Hassanein: Characterization of the spatial neutron distribution of the new beam line for cold neutron imaging ICON, PSI Project-Report P05074 (2005)
- [7] N. Frei: Dosisleistungsmessungen WNHA/ICON, PSI Strahlenschutz–Mitteilung (Juli 2005)
- [8] N. Frei: C-11 Messung mit und ohne Wolframharz, PSI Strahlenschutz–Mitteilung (November 2005)

# ***Two Eminent Members of the Swiss Neutron Society Receive the Walter Hälgl Prize of the European Neutron Scattering Association***

*J. Mesot*

*Laboratory for Neutron Scattering, PSI & ETH Zurich*

*5232 Villigen PSI, Switzerland*

At the last ICNS conference in Sydney, two members of the Swiss Neutron Society, Albert Furrer and Hans-Ulrich Güdel have been awarded the 5<sup>th</sup> Walter Hälgl<sup>(\*)</sup> Prize of the European Neutron Scattering Association (ENSA) in recognition of their many important contributions to our understanding of a wide variety of interesting magnetic materials. Before describing in some details their life-long joint and coherent activities and achievements, it is important to emphasize that through their respective universities (ETH Zurich) and (Univ. Bern) and their outstanding qualities as teachers, both Furrer and Güdel have been able to constantly recruit and maintain very competitive research teams, as can be seen from an impressive list of high-level publications.

The scientific co-operation between the groups of Furrer and Güdel can be considered as a truly interdisciplinary venture, because Furrer and Güdel received their university degrees in solid state physics and inorganic chemistry, respectively. Nevertheless, they achieved to combine and join the culture of the two disciplines in common projects with great success. Their co-operation started in the mid-seventies with studies of magnetic cluster compounds. They could directly measure the energy splittings of magnetic dimers and higher clusters by inelastic neutron scattering. Subsequently this work has served as a key reference in similar measurements performed by other groups, since it did not only demonstrate the feasibility of such experiments, but provided the theoretical basis for the data interpretation, as increasingly used today in the field of spin clusters including supramolecular nanomagnets.

Neutron experiments on magnetic clusters provide direct information on the exchange interaction between the magnetic ions. Up to the present, the Heisenberg model has been widely used to describe exchange interactions in magnetic systems, although it inherently represents just a first approximation of the true situation. Furrer and Güdel started to search for higher-order terms and found indeed direct spectroscopic evidence for an appreciable contribution of biquadratic exchange in neutron experiments on Mn pairs in the diluted one-dimensional magnet Cs(Mn,Mg)Br<sub>3</sub>. The nature of biquadratic exchange does not only involve pair interactions, but also three-body, four-body, etc...



Albert Furrer



Hans Ulrich Güdel

interactions if extended to higher clusters. Further neutron experiments on Mn trimer chain segments in  $\text{Cs}(\text{Mn}, \text{Mg})\text{Br}_3$  proved the existence of a true three-spin exchange term similar in magnitude to the corresponding biquadratic two-spin term. This was a result of fundamental importance, since  $n$ -body interactions ( $n > 2$ ) have so far only been verified in solid  $^3\text{He}$ , nuclear matter, and disordered binary alloys.

In the late eighties Güdel's group was searching for suitable materials to be used in the design of efficient up-conversion lasers. Compounds of composition  $\text{Cs}_3\text{R}_2\text{Br}_9$  ( $\text{R}$ =rare earth) were found to be particularly well suited for this purpose. The electronic properties of these compounds are governed by the dimers of  $\text{R}$  ions built into the molecular unit, thus it was obvious to study the corresponding excitations together with Furrer's group which had been active in  $\text{R}$  magnetism for a long time. The neutron experiments performed for almost the whole  $\text{R}$  series provided completely unexpected results. The usual phenomenological models (Heisenberg, Ising,  $xy$ ) failed to reproduce the observed energy spectra. However, an exchange-tensor formalism which takes into account the initial and final electronic states of the interacting ions, turned out to provide an excellent description.

A particularly interesting system studied by Furrer's and Güdel's groups was the spin-dimer compound  $\text{Cs}_3\text{Cr}_2\text{Br}_9$ , because it exhibits field-induced magnetic ordering when the singlet-triplet energy gap closes, thus Bose-Einstein condensation (BEC) of the triplet states with a gapless Goldstone mode could be expected to occur. However, detailed field-dependent neutron scattering experiments showed that the lowest singlet-triplet excitation branch does not soften completely due to some inherent anisotropy. Nevertheless, these experiments served as an excellent basis for the later observation of BEC in  $\text{TlCuCl}_3$ .

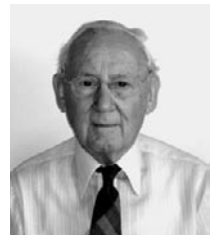
In the nineties Furrer's group started systematic investigations of the inhomogeneous materials properties of high-temperature superconductors. Motivated by the fact that

suitably doped spin-ladder compounds such as  $\text{Ca@Sr}_{14}\text{Cu}_{24}\text{O}_{41}$  become superconducting (under pressure), a co-operation was initiated for the novel  $S=1/2$  spin-ladder compounds  $\text{ACuCl}_3$  ( $A=\text{K, Tl, NH}_4$ ) with Güdel's group which has the necessary expertise in the synthesis and growth of single crystals. In a first step the dispersion of the magnetic excitations was established for  $\text{KCuCl}_3$  by inelastic neutron scattering. Surprisingly, the magnetic excitations turned out to be dispersive in all directions of reciprocal space (i.e., not only along the ladder direction as anticipated) with structure factors imaging the nearest-neighbour Cu pair distance, thereby proving that this compound series has the properties of an  $S=1/2$  spin-dimer rather than a spin-ladder compound. The experiments were then extended to investigate the magnetic field dependence of the singlet-triplet excitation including the isostructural compound  $\text{TlCuCl}_3$ . Based on these experiments Furrer, Güdel *et al.* realised that the field-driven quantum criticality can indeed be reached in these systems as demonstrated early 2003.

To conclude, Furrer's and Güdel's joint work over a period of three decades is exemplary. It demonstrates the virtues of inter-disciplinarity and continuity, and as such should be taken as a model for the younger generation of scientists.

**(\*) Prof. Walter Hälgl:**

The donator of the ENSA prize is Prof. Walter Hälgl, the founder of neutron scattering in Switzerland. Born in Basel in 1917, he is one of the pioneers of neutron scattering. From 1943 to 1946 he worked in particle physics at the Physical Institute of the University of Basel and on the construction of a 1 MeV Cockcroft-Walton accelerator. He spent the years 1946-1960 at the AG Brown Boveri Co Baden (BBC), and was promoted head of the physics department 1955. During his time at BBC, he worked on the development of the Swiss heavy water reactor DIORIT at Würenlingen, which went critical on 26 August 1960.



Walter Hälgl

Also in 1960, he was named full Professor for Nuclear Reactor Technology at the Swiss Federal Institute Zürich and was involved in the construction of the neutron spectrometers at the reactor DIORIT. He carried out the first calculations for a spallation source using the surplus protons of the 500 MeV ring of the near institute for neutron production, SIN, after decommissioning of the reactor DIORIT in August 1974.

During 10 years, he was member and president of the "Forschungskommission" of the Swiss Federal Institute Zürich. Currently, he is an honorary member of the Swiss Neutron Scattering Society and of the distinguished Physical Society of Zürich.

Walter Hälgl retired in autumn 1984.



## *2005 Walter Hälg Prize of the European Neutron Scattering Association (ENSA)*



Albert Furrer



Hans Ulrich Güdel

Every two years the European Neutron Scattering Association, ENSA, awards the prestigious Walter Hälg Prize to European scientists for an outstanding programme of research in neutron scattering with a long term impact on scientific and/or technical neutron scattering applications. The Prize of 10'000 Swiss Francs is donated by Professor Walter Hälg, the founder of neutron scattering science in Switzerland. In 2005 the Hälg Prize is to be presented at a special session of the International Conference on Neutron Scattering, to be held in Sydney, Australia, between November 27 and December 2.

The nominations received for the 2005 Hälg Prize were examined by an international selection committee consisting of authorities representing the major scientific disciplines, both within and beyond the field of neutron scattering. The selection committee is delighted to announce that the 2005 Hälg Prize will be awarded exceptionally to both

**Professor Albert Furrer (ETH Zürich and Paul Scherrer Institute)  
and  
Professor Hans Ulrich Güdel (University of Bern)**

in recognition of the important role their continuing collaboration has played in developing new and interesting magnetic materials and studying them to obtain unique

insights into their magnetic properties. The collaboration began in the 1970's with studies of magnetic cluster compounds that showed the detailed nature of the exchange interactions. The laser rare-earth materials were then studied and showed that the exchange interactions were more complex than expected, but could be understood by taking account of both the initial and final rare earth states. Most recently they have performed elegant experiments on spin dimers and have measured the triplet excitations and shown by applying a magnetic field that they could induce a Bose-Einstein condensation to a magnetically ordered state. All of these experiments show the importance of the collaboration between the chemist who grows the new materials and the neutron scatterer who studies the detailed nature of the excitations.

Albert Furrer obtained his doctorate at ETH, Zürich in 1970 and held post-doctoral positions in Denmark and the USA before returning to ETH, Zürich where he became Head of the Laboratory for Neutron Scattering from 1984-2004. He became Chairman of ENSA in 1997 and has held many important administrative posts.

Hans Ulrich Güdel obtained his doctorate from the University of Bern in 1970. He then went to Denmark and followed that by a time in Australia before returning to the University of Bern. He was co-founder and board member of the Swiss Neutron Scattering Association and has since held many important administrative roles in Neutron Scattering.

# Announcements

## SGN/SSDN Members

The Swiss Neutron Scattering Society welcomes the following new members:

- H. Sitepu, Department of Geosciences, Virginia Tech, Blacksburg, USA
- M. Janoschek, Laboratory for Neutron Scattering, PSI & ETH Zurich
- M. Salakhitdinova, Samarkand State University, Uzbekistan

Presently the SGN has 197 members.

## News from SINQ

During the annual accelerator shutdown of PSI in winter and spring 2006 the liquid lead bismuth target MEGAPIE will be installed at SINQ. Since the installation will cause an extended shutdown of the PSI neutron facility up to the end of June it was decided to cancel the fall 2005 call for proposals (deadline Nov 15). The waiting time between the submission of proposals and the schedule of beamtime would have been not acceptable for the users.

For the remaining operation cycle I/06 (July/August 06) the SINQ users are encouraged to make use of fast access procedures, for which an extended share of urgent beamtime will be reserved. The next regular call for proposals will be launched in spring 2006 asking for beamtime requests for the period September-December 2006. The users will be informed about important dates by an email newsletter.

*More information:*

<http://sinq.web.psi.ch/sinq/news.html>

<http://sinq.web.psi.ch/sinq/access.html>

<http://megapie.web.psi.ch>

## PSI Digital User Office also available for the $\mu$ S facility at PSI

Recently the PSI User Web interface 'Digital User Office, DUO' has been extended to host also the user operation of the Swiss Muon Source  $\mu$ S at PSI. In addition to SINQ and SLS, the  $\mu$ S is the third PSI user facility integrated into DUO. With a single

account the users now can submit proposals to the individual facilities, apply for PSI badges and dosimeters and manage their experiments at PSI.

*More information:*

<http://user.web.psi.ch/>

<http://sls.web.psi.ch/goto.php/duo/>

## **Open Positions at ILL**

To check the open positions at ILL please have a look at the ILL-homepage: <http://www.ill.fr> following the link 'Job Offers'.

# *4<sup>th</sup> Summer School on Condensed Matter Research, Zuoz, Switzerland*

*F. van der Veen and H.J. Weyer  
Swiss Light Source, Paul Scherrer Institut, 5232 Villigen PSI, Switzerland*

The Paul Scherrer Institut offers world-class synchrotron, neutron, and muon facilities. For the 2005 Zuoz Summer School, therefore, “Spectroscopy/Microscopy” was chosen as main topic. Following the concept of the school, also noted in the announcement, no special knowledge of the field was required.

Accordingly, the program started with basic introductions to the generation of synchrotron radiation (Leonid Rivkin) and neutrons (Kurt Clausen) and scientific questions addressed at these facilities (Friso van der Veen, Joel Mesot). This concept of tandem talks (one talk emphasizing the technique, the other scientific applications) was followed throughout the program. Philipp Aebi presented the basics of angle-resolved photoemission or  $k$ -space microscopy and Mark Golden elucidated its applications in the field of high- $T_c$  superconductors.

Resonant inelastic X-ray scattering was covered by Marco Grioni and Giacomo Ghiringhelli, with a description of the technique, instrumentation, and selected experimental results using soft and hard X-rays. Applications of this technique to strongly correlated materials under high pressure were discussed by Claudia Dallera. Neutron



Zuoz village tour during an afternoon break.

spectroscopy as a probe of structural and magnetic dynamics was introduced by Andrew Boothroyd. Des McMorrow discussed excitations in condensed matter probed with neutrons.

As there is also a powerful muon-spin-rotation ( $\mu$ SR) facility at PSI, Christof Niedermayer discussed what muons can tell us about condensed matter, by pointing to their strong sensitivity to local magnetic fields and their temporal fluctuations.

A strong and ever-increasing community at synchrotron facilities uses the technique of X-ray Absorption Fine Structure (XAFS). Its wide applicability in materials and environmental sciences and its sensitivity to short-range ordering was discussed by Roel Prins and Donald Sparks.

Infrared spectroscopy with its different facets was presented by Leo Degiorgi and Mark Tobin, while Michael Martin introduced the audience to the possibility of using Terahertz radiation at synchrotron facilities. The use of infrared ellipsometry for the characterization of superconductors was elucidated by Dirk van der Marel. The options of X-ray microscopy with its elemental and chemical sensitivity were discussed by Harald Ade. Rainer Fink discussed applications of zone-plate based x-ray transmission microspectroscopy.

Photoelectron emission microscopy used as a probe of magnetism on the nanoscale was described by Frithjof Nolting. Maya Kiskinova described the approach to chemical and electronic properties of surfaces and interfaces. Thomas Greber gave an impressive insight into the potential applications of photoelectron diffraction and Urs Staub took the audience on the road from ordered charge to ordered orbitals. He demonstrated that by resonant scattering, i.e., by combining spectroscopy with diffraction, the orientation of the orbitals can be probed.

According to the style of the meeting as a school, basic issues should not be forgotten. Claus Ascheron gave in his talk an introduction to scientific presentation and discussed those issues essential for giving a good scientific talk. Although directed mainly toward the younger participants, the talk was definitely also of interest for the more senior attendees. The meeting concluded with a discussion of magnetic excitations in strongly correlated systems by Stephen Hayden.

The school was attended by over one hundred participants, among them about eighty students on the post-graduate or post-doctoral level. The majority of these students came from western- and eastern European countries. Transparencies of the presentations were made available to the participants during the school. PDF versions of the talks have been deposited on the school website (<http://sls.web.psi.ch/view.php/science/events/Conferences/Zuoz2005/Program.html>).

We thank Mrs Christine Kunz for all the arrangements she made that turned the school in a success. The support of the school by the EU FP6 I3 Initiatives IA-SFS and NMI3 and by the Swiss National Science Foundation is gratefully acknowledged.

## *‘Day of Physics’ at PSI on October 30*

*S. Janssen*

*NUM department, Paul Scherrer Institut, 5232 Villigen PSI, Switzerland*



More than 9000 visitors attended the ‘PSI Day of Physics 2005’.

On October 30, 2005 the Paul Scherrer Institut opened its doors for another visitors’ day and faced an overwhelming interest of the public: More than 9000 people took the opportunity to have a closer look at the PSI facilities and research laboratories during the ‘Day of Physics’.

On their way over the campus the visitors passed by four ‘Einstein-Presentations’ entitled ‘Light’, ‘Space and Time’, ‘Energy’ and ‘Atoms’. In multimedia shows the people were intro-

duced to topics like ‘speed of light,  $E=mc^2$ , photo effect’ or ‘diffusion’.

In addition the PSI User Laboratories SLS, SINQ,  $\mu$ S, and the particle physics presented their methods and hot research topics in a public manner. At SINQ the presentation showed how neutrons might help to explain the effect of High-Temperature Superconductivity. A special highlight during the ‘show’ was the superconducting ‘MANEP model railway’, which was kindly made available by the Institute of Physics, University of Geneva.

The PSI/Michelin fuel cell car ‘HY-LIGHT’, the PSI proton therapy facility, several information booths on energy research and environment as well as a special ‘physics laboratory for children’ completed a very interesting, colorful and lively ‘Open Day’ at PSI, which will definitely not be the last one.



Even ‘Einstein’ showed up to examine if his theories are really understood...

# *Conferences and Workshops 2006*

*(an updated list with online links can be found here: <http://sinq.web.psi.ch/sinq/links.html>)*

## **January**

Innovative Nanoscale Approach to Dynamic Studies of Materials  
*January 9-14, 2006, Okinawa, Japan*

Gordon Research Conference (GRC) on Superconductivity  
*January 22-27, 2006, Santa Ynez Valley Marriott Buellton, CA, USA*

High Pressure PSI Workshop:  $\mu$ SR Techniques and Applications  
*January 25, 2006, Paul Scherrer Institute, Villigen, Switzerland*

S $\mu$ S Users' Meeting  
*January 25-26, 2006, PSI Villigen, Switzerland*

## **February**

2006 Swiss Physical Society - MaNEP Symposium  
*February 13-14, 2006, EPFL Lausanne, Switzerland*

Workshop on 'Present Status and Future of Very Cold Neutron Applications'  
*February 13-14, 2006, Paul Scherrer Institut, Switzerland*

Symposium for the Inauguration of the 'Juelich Centre for Neutron Science JCNS'  
and European Users Meeting  
*February 16-17, 2006, Forschungszentrum Jülich, Germany*

## **March**

Swiss-Russian Workshop on 'Quantum Magnetism and Polarised Neutrons'  
*March 1-4, 2006, PSI Villigen, Switzerland*

10<sup>th</sup> Laboratory Course on Neutron Scattering  
*March 13-24, 2006, FZ Jülich, Germany*

Confit2006 – 3<sup>rd</sup> International Workshop on Dynamics in Confinement  
*March 23-26, 2006, Grenoble, France*

Spring Meeting (Solid State Physics) of the German Physical Society and EPS  
Condensed Matter Division  
*March 27-31, 2006, Dresden, Germany*

## **April**

14<sup>th</sup> Annual Meeting of the German Crystallographic Society  
*April 3-6, 2006, Freiburg, Germany*

ILL Millenium Symposium and European Users Meeting  
*April 27-29, 2006, ILL Grenoble, France*

## **May**

8<sup>th</sup> SINQ Users' Meeting  
*May 10, 2006, PSI Villigen, Switzerland*

ICCS 2006: International Conference on Computational Science  
*May 28-31, 2006, University of Reading, UK*

## **June**

11<sup>th</sup> International Ceramic Congress and 4th Forum on New Materials  
*June 4-9, 2006, Acireale, Sicily, Italy*

European School on 'Scattering Methods applied to Soft Condensed Matter'  
*June 10-17, 2006, Bombannes, Gironde, France*

IFAMST 5: 5th International Forum on Advanced Material Science and Technology  
*June 11-17, 2006, Xiangtan and Zhangjiajie, Hunan Province, China*

2006 American Conference on Neutron Scattering  
*June 18-22, 2006, St. Charles, IL, USA*

## **July**

Strongly correlated systems in low dimension  
*July 2-8, 2006, Ascona, Switzerland*

XIII International Conference on Small Angle Scattering  
*July 9-13, 2006, Kyoto, Japan*

M2S-HTSC-VIII, 8th International Conference on Materials and Mechanisms of Superconductivity and High Temperature Superconductors

*July 9-14, 2006, Dresden, Germany*

ACA 2006, Annual Meeting of the American Crystallographic Association 2006

*July 22-27, 2006, Honolulu, Hawaii, USA*

## **August**

5th PSI Summer School on Condensed Matter Research

*August 19-26, 2006, Zuoz, Switzerland*

## **September**

10<sup>th</sup> European Powder Diffraction Conference

*September 1-4, 2006, Geneva, Switzerland*

IC fe 2006: 6th International Conference on f-elements

*September 4-9, 2006, Wroclaw, Poland*

7<sup>th</sup> European Conference on Residual Stresses

*September 13-15, 2006, Berlin, Germany*

Polarised Neutron School

*September 19-22, 2006, Berlin, Germany*

PNCMI 2006, Polarised Neutrons in Condensed Matter Investigations

*September 25-28, 2006, Berlin, Germany*

